

X- and C-Band SAR Surface Displacement for the 2013 *Lunigiana* Earthquake (Northern Italy): A Breached Relay Ramp?

Salvatore Stramondo, *Senior Member, IEEE*, Paola Vannoli, Valentina Cannelli, Marco Polcari, Daniele Melini, Sergey Samsonov, Marco Moro, Christian Bignami, *Member, IEEE*, and Michele Saroli

Abstract—In this paper, we applied the differential interferometric synthetic aperture radar (DInSAR) technique to investigate and measure surface displacements due to the M_w 5.3 (M_l 5.2), June 21, 2013 earthquake, occurred north of the Apuan Alps (NW Italy), in the discontinuity zone between the Lunigiana and Garfagnana area. Two differential interferograms showing the coseismic displacement have been generated using X-band and C-band data, taken from COSMO-SkyMed and RADARSAT-2 satellites, respectively. Both interferograms highlighted a clear pattern of subsidence of few cm located between the Lunigiana and Garfagnana basins. We then modeled the observed SAR deformation fields using the Okada analytical formulation and found them to be consistent with an extensional fault plane dipping toward NW at about 50° . The integrated analysis of DInSAR, geological data, modeling, and historical seismicity suggest that the fault responsible for the June 2013 earthquake corresponds to a breached relay ramp connecting the Lunigiana and Garfagnana seismogenic sources.

Index Terms—Earthquakes, inversion modeling, normal fault, relay ramp, remote sensing, seismogenic source, surface displacement.

I. INTRODUCTION

THE NORTHERN Apennines are affected by the northwestern prolongation of the Etrurian Fault System (EFS), a NW-SE trending normal fault system, which extends for about 350 km from Umbria to Tuscany [1]. Historical and instrumental seismicity in the northwestern termination of the EFS, hereafter the Lunigiana and Garfagnana area, testify that it is an active and seismogenic zone. The fault responsible for the strongest earthquake of this region, the 1920 earthquake (M_w 6.5), is a segment of this regional fault system [2], about 18 km long. Most of the largest ($M > 5$) historical earthquakes are located close to the transfer zone [3] of the EFS, between the extensional Lunigiana (to northwest) and the Garfagnana (to southeast) basins.

Manuscript received December 09, 2013; revised March 18, 2014; accepted March 21, 2014. Date of publication May 19, 2014; date of current version August 21, 2014.

S. Stramondo, P. Vannoli, V. Cannelli, M. Polcari, D. Melini, M. Moro, and C. Bignami are with Istituto Nazionale di Geofisica e Vulcanologia, 00143 Rome, Italy (e-mail: salvatore.stramondo@ingv.it).

S. Samsonov is with Canada Centre for Mapping and Earth Observation, Natural Resources Canada, Ottawa, ON K1S 5K2, Canada.

M. Saroli is with the Department of Civil and Mechanical Engineering, University of Cassino and Southern Lazio, 03043 Cassino, Italy.

Color versions of one or more of the figures in this paper are available online at <http://ieeexplore.ieee.org>.

Digital Object Identifier 10.1109/JSTARS.2014.2313640

Here, we present the outcomes concerning the June 21, 2013, M_w 5.3 *Lunigiana* earthquake, occurred in such discontinuity zone, during an ongoing seismic sequence. We inverted the surface displacement field stemmed from synthetic aperture radar (SAR) in order to retrieve the geometry, kinematics, and the slip distribution of the seismic source. Such analyses allowed us to characterize the accommodation of extension between the Lunigiana and Garfagnana normal fault segments.

II. SEISMOTECTONIC FRAMEWORK

On June 21, 2013 (10:33 UTC), an M_w 5.3 (M_l 5.2) event has been located at about 5 km depth, north of the Apuan Alps, a mountain range of the Northern Apennines [4] (Fig. 1). The main event was preceded by a foreshock on June 15 (M_l 3.4), and has been followed by more than 2450 aftershocks with a maximum magnitude of 4.4. The whole sequence is located toward NE of the mainshock [4]. The area affected by the seismic sequence is in Tuscany region, between the Lunigiana area to NW and the Garfagnana to SE. The mainshock was felt over a broad area in Northern Italy (if compared with its magnitude) [5], but with minor damage in the epicentral area (maximum intensity VI MCS) [6].

The focal mechanism of the main event and of its aftershocks suggests that slip occurred along a $\sim 45^\circ$ dipping fault plane, with a prevailing extensional sense of motion [7]–[10].

The Lunigiana and Garfagnana area is historically characterized by a dense intermediate to damaging seismicity (Fig. 1). On April 11, 1837 an M_w 5.8 earthquake occurred north of the Apuan Alps, causing severe damage in Minucciano village and its surroundings (IX MCS intensity) and was felt over a broad region reaching up the Po Plain [11], [12]. The strongest earthquake known in this region occurred on September 7, 1920 (M_w 6.5) and reached a very high epicentral intensity (X MCS), devastating a wide area of Garfagnana and Lunigiana [11], [12]. Moreover, on October 15, 1939, an M_w 4.8 earthquake occurred about 10 km to the northeast of the June 21, 2013 event [12]. More recently, on October 10, 1995, an M_w 5.1 earthquake of with strike-slip kinematics [13]–[15] occurred about 10 km to the southwest of the 2013 seismic sequence.

From a geological point of view, Lunigiana and Garfagnana regions are characterized by a marked complexity due to the coexistence of different geological structures and by the presence of superimposed tectonic units, particularly the metamorphic and

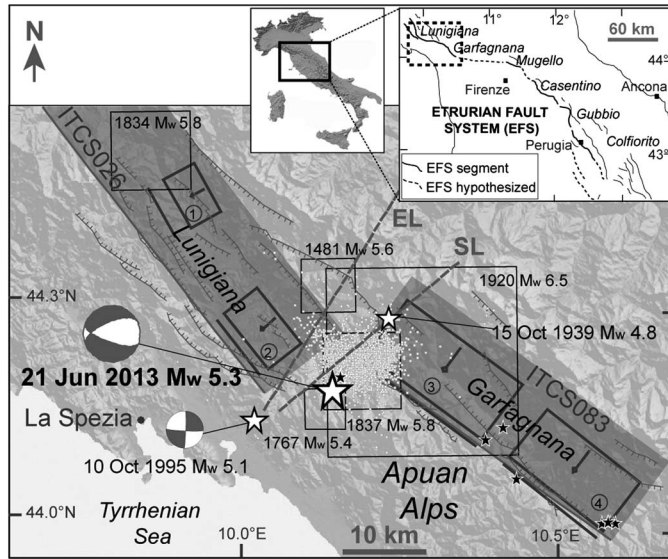


Fig. 1. Structural sketch of the Lunigiana and Garfagnana area with the June 21, 2013 earthquake, its focal mechanism (<http://cnt.rm.ingv.it/tfmt.html>) and the 2013 sequence [4]. Squares: historical earthquakes having magnitude larger than 5.3 [12]; hatched lines: normal faults [21]; dashed lines: lineaments, EL: Enza line [23], SL: Sarzana-Equi Terme line [3]; dark polygon: composite seismogenic sources projection on the ground surface, black boxes: individual seismogenic sources projection onto the ground surface; black lines: up-dip projection of the seismogenic sources onto the surface 1) ITIS085-Pontremoli; 2) ITIS067-Aulla; 3) ITIS050-Garfagnana North; and 4) ITIS051: Garfagnana South [2]; black stars: thermal springs. Inset shows the structural framework of the Etrurian Fault System (redrawn from [1]).

nonmetamorphic Tuscan Succession, the Apuan Alps structure and the Ligurian units. These units are overlying by Pliocene to Holocene lacustrine and fluvial deposits [16]. The Lunigiana and Garfagnana areas are the northwestward termination of the regional, NW-SE trending EFS, marking the northwestern extensional border of the Northern Apennines. The NE dipping, low-angle normal EFS is rather well known in the literature due to field data and seismic reflection profiles (e.g., [1], [17]). The EFS straddles the northern Apennines for about 350 km and, south of the study area, include the Mugello, Casentino, and Tiber extensional basins (inset in Fig. 1; [18]). Historical and recent seismicity show that two seismogenic normal faults border the Lunigiana and Garfagnana basins (respectively, ITCS026 and ITCS083 composite seismogenic sources in Fig. 1; e.g., [19], [2]). The Lunigiana ITCS026 Source extends for about 50 km to the northern side of the Apuan Alps. Two individual sources (IDs 1 and 2 in Fig. 1) are part of this Composite Source (e.g., [20], [21]), and are believed to be responsible for the 1834 and the 1481 earthquakes, respectively [2]. The Garfagnana ITCS083 source extends for about 40 km to the eastern side of the Apuan Alps, and is left-stepped compared to the Lunigiana. Also, the Garfagnana includes two individual sources [21]: 1) the source responsible for the destructive 1920 earthquake (ID 3; Fig. 1); 2) the southeastern source (ID 4; Fig. 1) not associated with a known historical or instrumental earthquake, whose existence is based on geological and structural evidence [2]. Between the Lunigiana and Garfagnana sources there is a complex and poorly known shear zone that locally forms the northern boundary of the Apuan Alps. Here falls the Equi Terme thermal spring (temperature about 24°C), probably because the transfer zone enables

water to reach deeper portions of the crust [22]. This zone is affected by two key transversal structures, inferred from remote sensing data and surface geology, known in the literature as the NE-SW trending Sarzana-Equi Terme Lineament (SL in Fig. 1) and the NNE-SSW trending Enza Lineament (EL in Fig. 1). The SL has been interpreted as a normal fault with a left-lateral slip component [3], the EL as a left-lateral strike-slip fault [23]. Furthermore, this zone has been interpreted even as an EW active normal-oblique right-lateral transfer fault, connecting the NE-dipping Lunigiana and Garfagnana sources [18]. The above-mentioned works highlight that different structural interpretation for this zone are available; in addition, the evidence of its activity proposed in the literature have few constraints.

III. DInSAR PROCESSING AND RESULTS

We have investigated the surface displacement field due to the Lunigiana earthquake by exploiting a multiband SAR dataset, coming from COSMO-SkyMed (X-band, hereafter CSK) and RADARSAT-2 (C-band, hereafter RDR) SAR satellites (Fig. 2), at high spatial resolution (3–10 m pixel).

DInSAR technique is based on the exploitation of the phase component of two SAR images [24]. Today DInSAR is used in a wide range of fieldworks, from seismology [25], to volcanology [26], to urban subsidence [27] and infrastructures monitoring [28]. Phase component is related to the satellite-to-target distance and the result of the application of this technique is called interferogram. The interferometric phase φ_{int} can be schematically split into five terms: 1) the “flat Earth” component φ_f ; 2) the topographic phase φ_{topo} ; 3) the displacement phase φ_{displ} ; 4) the atmospheric term φ_{atm} ; and 5) the error phase φ_{err} [24]. The first two components can be removed easily by exploiting the orbital satellite data and by using an external digital elevation model (DEM), respectively. The atmospheric contribution and phase errors are usually neglected in coseismic interferograms being relatively lower than the displacement phase. The phase variation due to displacement (φ_{displ}) provides a map of sensor-to-ground distance change at pixel scale.

The first image pair was acquired by the CSK constellation, an Earth observation mission developed by the Italian Space Agency (ASI), consisting of a four-satellite system equipped with high-resolution X-band SAR sensors. The second image pair was acquired by the Canadian RDR satellite equipped with high-resolution C-band sensor. These satellites image Earth surface in various acquisition modes, with different ground resolutions, incidence angles and polarizations [29], and provide global coverage independent on weather or lighting conditions.

The X-band CSK sensor imaged the epicentral region on June 21 (before the mainshock) and June 22, 2013 with a spatial baseline of 139 m along the ascending orbit. The 1-day time span is the minimum temporal interval ensured by the CSK constellation. Such a short time span minimizes temporal decorrelation that heavily affects the study region due to steep topography and dense vegetation coverage. The $40 \times 40 \text{ km}^2$ (Stripmap-mode) CSK pair observed the surface with 40° incidence angle and was centered on the village of Minucciano. To improve the signal-to-noise ratio, the multilook factor was set equal to 20 in order to obtain a square pixel representing an area of about $40 \times 40 \text{ m}^2$.

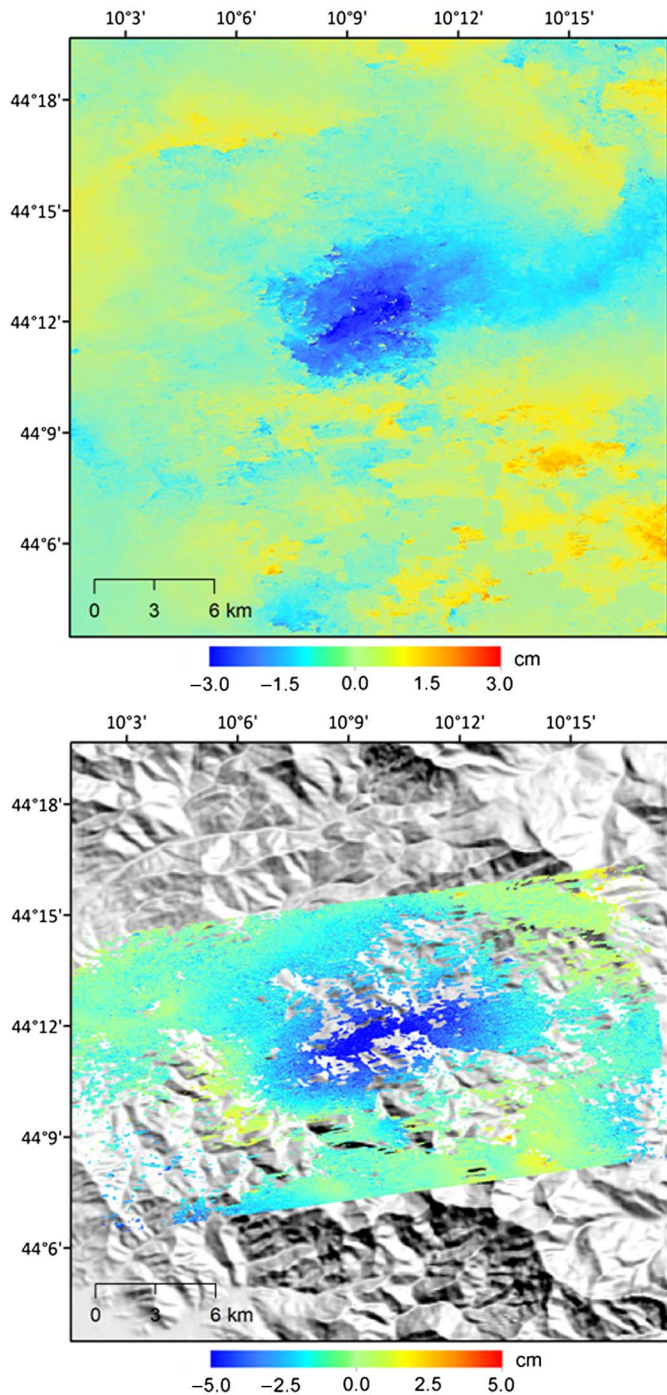


Fig. 2. Surface displacement detected by COSMO-SkyMed (upper) and RADARSAT-2 (bottom) DInSAR. The apparent discrepancy between the results can be ascribed to the different temporal baseline (1-day delay for COSMO-SkyMed, 24 days for RADARSAT-2) that implies additional deformation due to aftershocks and post-seismic slip release.

The C-band RDR imaged the epicentral region on June 18 and July 12, 2013 with a Standard-3 (S3) beam with 69 m spatial baseline along the ascending orbit. The RDR pair observed a $100 \times 100 \text{ km}^2$ surface with 34° incidence angle.

The interferometric processing was performed with the GAMMA software [30]. The 90 m shuttle radar topographic mission (SRTM) DEM was used to remove topographic component from COSMO-SkyMed interferogram and 30 m ASTER

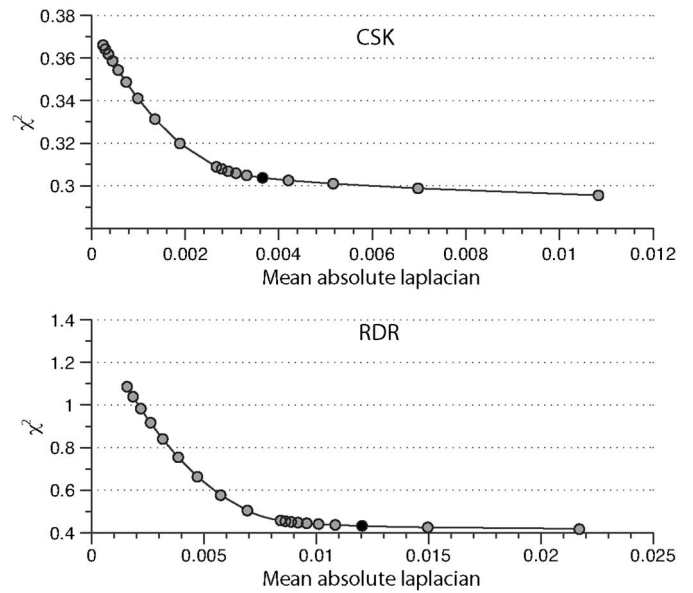


Fig. 3. Misfit-roughness tradeoff curves for the CSK (top) and RDR (bottom) models. Each gray dot corresponds to a different value of the weighting factor of the smoothing operator. A black dot marks the weighting factor used for presented results.

TABLE I
SOURCE MODEL PARAMETERS RESULTING FROM THE UNIFORM-SLIP INVERSION

	CSK	RDR
Center longitude	10.19 E	10.18 E
Center latitude	44.22 N	44.20 N
Top depth (km)	2.9	2.4
Strike ($^\circ$)	244	247
Dip ($^\circ$)	52	50
Rake ($^\circ$)	-84	-87
Slip (m)	0.09	0.16
Length (km)	9.3	6.8
Width (km)	6.5	6.7

DEM was used to remove the topographic component from RADARSAT-2 interferogram. The Goldstein filtering [31], phase unwrapping with minimum cost flow (MCF) algorithm [32] and orbital refinement were also applied to both interferograms. The results obtained from CSK data show a surface subsidence of about 3 cm in the satellite line-of-sight (LOS). This displacement is mainly due to the mainshock thanks to the short temporal baseline of 1 day. On the other hand, the larger RDR temporal baseline of 24 days results in a more pronounced subsidence of about 5 cm in the satellite LOS probably caused by the cumulated effect of aftershocks following the June 21 event and/or by postseismic deformation.

IV. SOURCE MODELING

We used the coseismic deformation fields imaged by DInSAR to infer the seismic source characteristics through an inverse modeling analysis, using analytical expressions from Okada [33] to compute expected deformation and assuming an homogeneous

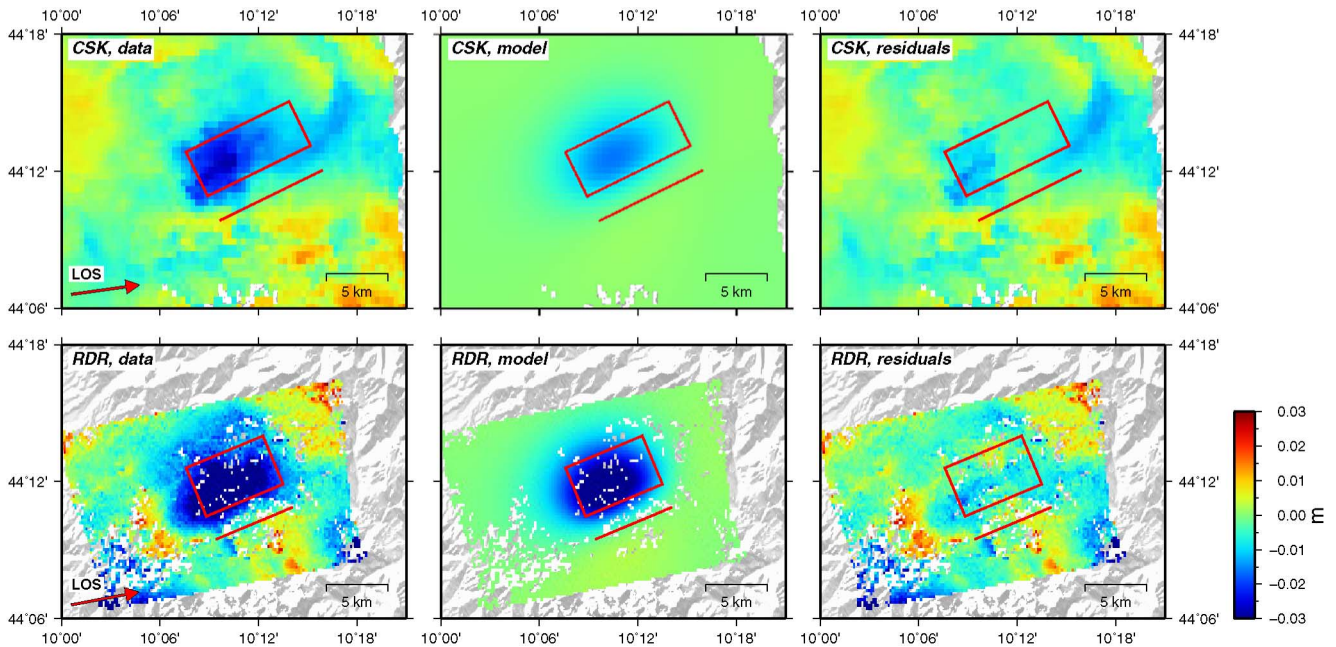


Fig. 4. Unwrapped LOS InSAR deformation (left), modeled deformation field (center) and residuals (right) for the CSK and RDR datasets. The red box marks the position and surface projection of the best-fitting uniform slip model. LOS indicates the satellite view direction (red arrow in left panels).

half-space with elastic constants corresponding to a Poisson solid. As discussed above, while the CSK interferogram is obtained from a pair of images acquired on two consecutive days, RDR interferogram has a much longer temporal baseline (24 days). Therefore, it is likely that the deformation field from RDR includes the contribution of the aftershocks in the sequence as well as short-term postseismic effects. For this reason, instead of a joint modeling of the two fields, we chose to independently compute a source model for each deformation field and compare the results.

The source geometry is obtained as the result of a two-step inversion process. First, we estimate geometry, location, and extents of the fault with a nonlinear optimization scheme, assuming uniform slip on the fault plane. Once the fault geometry is fixed, we obtain the best-fitting slip distribution on the fault plane by means of a linear inversion.

In the first step, we obtained a best-fitting uniform-slip source geometry by minimizing the chi-square between the observed field and the projection of the three components of the modeled field on the satellite LOS direction [34]. The fault geometry that minimizes the misfit function is obtained as the result of a nonlinear inversion with the Simulated Annealing algorithm [35]. For computational reasons, the dataset used for each inversion is a subsample of the original one, with about 10% of the total pixels. We checked the stability of each solution by using it as a starting point for a gradient-descent optimization, and verified that we recovered the original model.

To obtain the slip distribution in the second step of the inversion, we subdivided the fault geometry resulting from the nonlinear step into square patches of about $0.5 \times 0.5 \text{ km}^2$, and composed a Green Function matrix by imposing a unitary slip on each patch, computing the corresponding deformation field according to the Okada analytical expressions [33] and

projecting it onto the satellite LOS direction [34]. We included in the Green Function matrix a discrete approximation of the Laplacian operator in order to avoid large, unphysical oscillations in the slip values; the linear problem is then solved by computing a natural inverse with the singular-value decomposition (SVD) algorithm, applying a damping factor in order to correct singularities in the data kernel [36]. When applying a smoothing term to exclude unphysical oscillations of the slip, a tradeoff is introduced between data misfit and solution roughness. We calibrated the weight of the smoothing factor by computing several inversions varying values of the Laplacian weight, and setting the smoothing parameter at the “knee” of the resulting misfit-roughness curve (Fig. 3).

The best-fitting source parameters are listed in Table 1 for the two datasets, whereas the modeled deformation fields are shown in Fig. 4, and the estimated slip distribution on the two source models is displayed in Fig. 5. The strike, dip, and rake angles turn out to be very similar for the two inversions and indicate that rupture occurred on a normal fault dipping toward NNW at about 50° . This geometry is consistent with RCMT and TDMT solutions, which give an extensional rupture with dip in the range $41\text{--}47^\circ$. Depth extension is 2.4–7.5 km for the RDR model and 2.9–8.0 km for the CSK model. The fault models have comparable along-dip width, whereas length of the CSK model is about 50% larger than RDR model. Peak slip for the CSK model (8.8 cm) occurs at 5.1 km depth, whereas in the RDR model peak slip (19.4 cm) is at 3.8 km depth. Geodetic magnitude for the CSK and RDR sources are M 5.24 and M 5.40, respectively, if a crustal rigidity of 26 GPa is assumed.

The spatial resolution of the inverted slip distribution has been estimated by defining a synthetic slip model with a checkerboard pattern, computing the corresponding deformation field with the same coverage of SAR data and inverting it through the same procedure used for the real datasets. Results are shown in

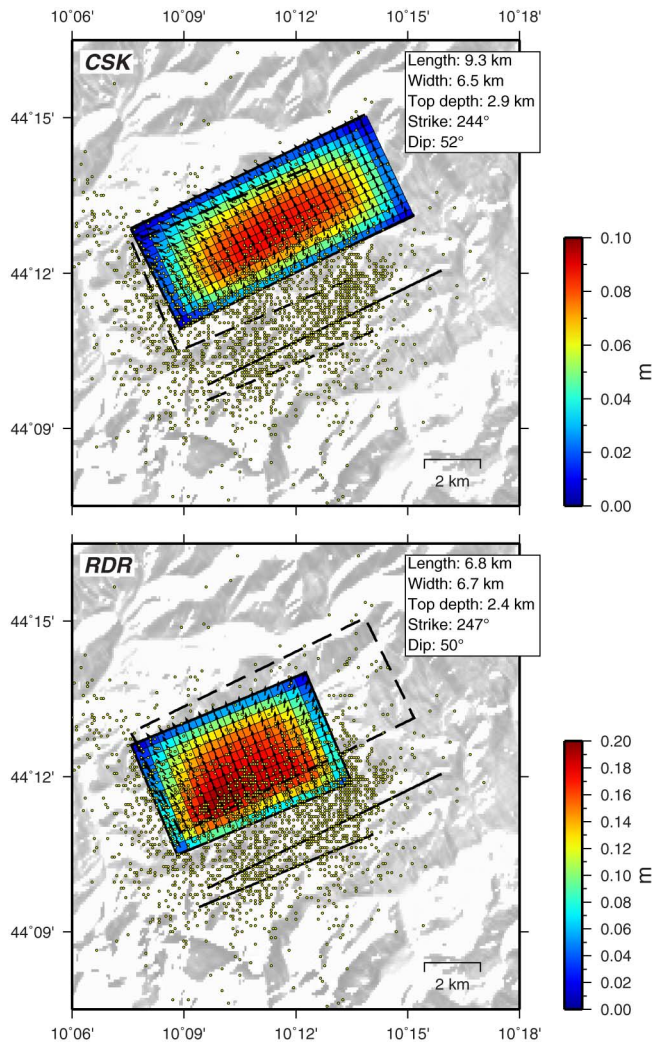


Fig. 5. Slip distribution models obtained with the CSK (top) and RDR (bottom) datasets. The extents and surface projection of the two source models are shown in both panels for comparison. Yellow dots show seismicity from June 21, 2013 to October 23, 2013. Color scale for the two models are different to account for the larger amount of slip in the RDR model, as a consequence of the larger temporal baseline in the RDR deformation field.

Fig. 6(a) and (b) for the CSK and RDR models, respectively. Spatial resolution decreases with depth, as expected in geodetic inversions (e.g., [37]), and in the shallower half of the fault it can be estimated as about 4 km.

The empirical relations of Wells and Coppersmith [38] applied to a normal mechanism with moment magnitude M_w 5.3 estimate a subsurface rupture length of 5.3 km and a rupture width of 4.8 km. Uniform slip models have larger extents for both datasets (Table 1); however, if we consider the extents of the bulk slip area in Fig. 5 as the effective rupture size, both CSK and RDR models are compatible with a 25 km^2 rupture area obtained from empirical relationships. A rupture area with this size should be within the spatial resolution of the models, at least in the shallower portion of the fault [Fig. 6(a) and (b)]. The geodetic magnitude of the CSK model (M 5.24) is in excellent agreement with seismological magnitudes, whereas the RDR model overestimates the magnitude and gives twice the peak slip of the CSK model. Such discrepancy can be ascribable, as

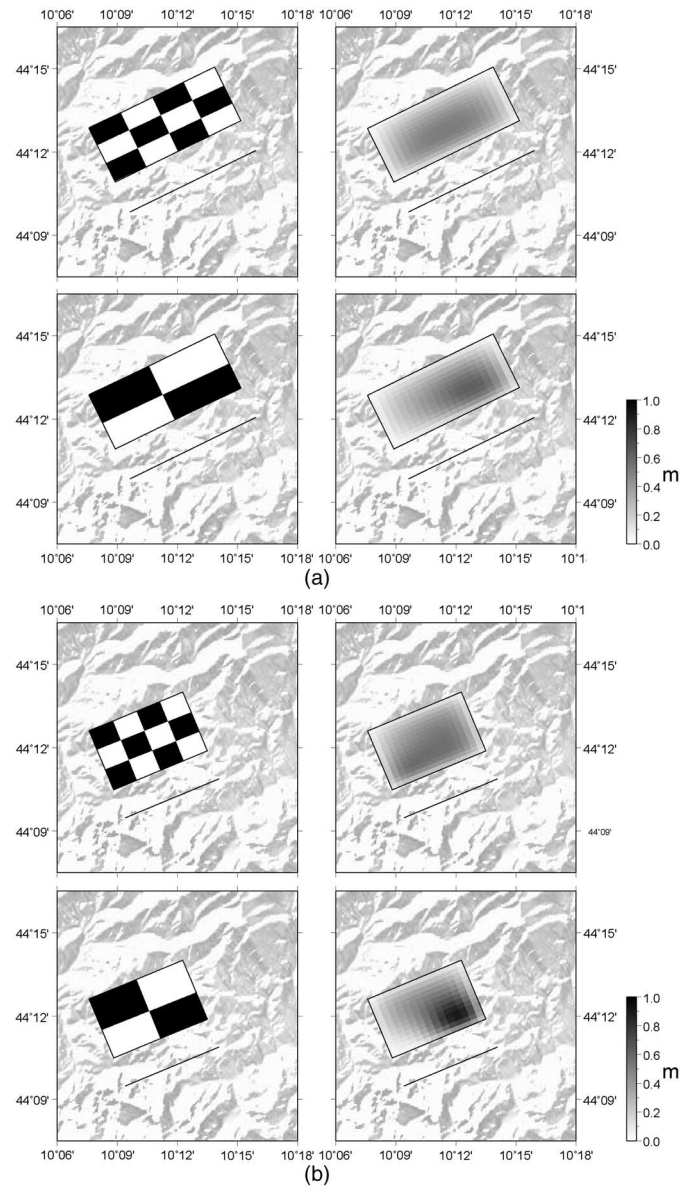


Fig. 6. (a) Resolution tests for the CSK model. Synthetic and inverted models are shown in the left and right panels, respectively. Checkerboard patch size is about $4.5 \text{ km} \times 3 \text{ km}$ in the bottom panels and $2 \text{ km} \times 2 \text{ km}$ in the top panels. (b) Resolution tests for the RDR model. Synthetic and inverted models are shown in the left and right panels, respectively. Checkerboard patch size is about $3.5 \text{ km} \times 3 \text{ km}$ in the bottom panels and $1.8 \text{ km} \times 2 \text{ km}$ in the top panels.

already mentioned, to the larger temporal baseline (24 days) of the RDR pair, with the result that the measured deformation includes short-timescale postseismic motions as well as the cumulated effect of minor shocks occurred during the time window [39]. Indeed, during the whole RDR acquisition window, four events with $M_l \geq 4.0$ occurred: two (of M_l 4.0) in the same mainshock date and very near to it and two (of M_l 4.4) at the end of June. The cumulated seismic moment release of the sequence in the RDR acquisition window is $1.81 \times 10^{17} \text{ Nm}$, corresponding to a moment magnitude M_w 5.47. The geodetic magnitude of the RDR model is close to the cumulated magnitude of the sequence, so we can conclude that the deformation field measured by RDR is likely to include the

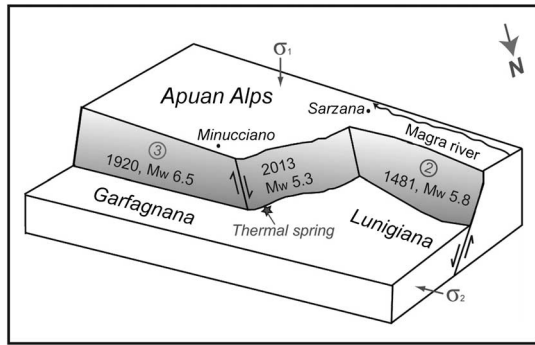


Fig. 7. Block diagram with the simplified fault geometry of the Lunigiana and Garfagnana areas. The source responsible for the 1920 earthquake (ID 3—Garfagnana North Source, see also Fig. 1) is schematically linked to the source responsible for the 1481 earthquake (ID 2—Aulla Source) by the relay ramp hosting the June 21, 2013 fault. Notice the presence of the Equi Terme thermally anomalous spring.

contribution of minor aftershocks occurred between the acquisition dates.

V. CONCLUSION

In this study, we have exploited the capabilities of CSK and RDR in terms of very high spatial resolution and short (in case of CSK) revisit time. The availability of two SAR datasets, from two different sensors (at X- and C-bands) has allowed to have a stronger constraint to the deformation pattern. Furthermore, we have integrated seismotectonic and geological data with DInSAR results to characterize a transfer zone connecting the Lunigiana and the Garfagnana basins.

In order to provide an analysis of the June 2013 earthquake, we have applied an inversion modeling algorithm exploiting as input data the surface deformation field from DInSAR. It should be noted that the M_w 5.3 of the June 2013 Lunigiana earthquake roughly coincides with a rupture length that is close to the limit of resolution of any method of geologic investigation of earthquake faulting.

One of the outcomes of our model is the positioning of the source responsible for the June 21 earthquake within the transfer zone. Furthermore, concerning the geometry and kinematics of the fault, we defined an NE-SW trending, NW dipping (about 50°), normal fault.

Our study has pointed out the structural style of linkage between the Lunigiana and Garfagnana fault segments. We thus lean toward identifying a breached synthetic relay ramp [40] (Fig. 7).

It can be noted how the integrated analysis of different data sources (DInSAR, geological data), together with the historical seismicity (1767 M_w 5.4 and 1837 M_w 5.8 earthquakes), suggests that the relay ramp between Lunigiana and Garfagnana is a seismogenic structure potentially responsible for earthquakes larger than M_w 5.3.

ACKNOWLEDGMENT

The authors thank the Italian Space Agency (ASI) for providing CSK data and the Canadian Space agency for RDR data.

REFERENCES

- [1] P. Boncio, F. Brozzetti, and G. Lavecchia, "Architecture and seismotectonics of a regional low-angle normal fault zone in Central Italy," *Tectonics*, vol. 19, pp. 1038–1055, 2000.
- [2] DISS Working Group. (2010). *Database of Individual Seismogenic Sources (DISS), Version 3.1.1: A Compilation of Potential Sources for Earthquakes Larger than M 5.5 in Italy and Surrounding Areas* [Online]. Available: <http://diss.rm.ingv.it/diss/>, doi: 10.6092/INGV.IT-DISS3.1.1.
- [3] M. Boccaletti, M. Coli, and G. Napoleone, "Nuovi allineamenti strutturali da immagini Landsat e rapporti con l'attività sismica negli Appennini," *Boll. Soc. Geol. Ital.*, vol. 96, pp. 679–694, 1977.
- [4] ISIDe Working Group. (2013). *Italian Seismological Instrumental and Parametric Database* [Online]. Available: <http://iside.rm.ingv.it>
- [5] INGV (2013). [Online]. Available: www.haisentitoilterremoto.it
- [6] QUEST. (2013). *Quick Earthquake Survey Team* [online]. Available: <http://quest.ingv.it/it/rilievi-macrosismici.html>
- [7] GFZ. (2013). *GEOFON Moment Tensor Solutions* [Online]. Available: <http://geofon.gfz-potsdam.de/eqinfo/list.php?mode=mt>
- [8] Moment Tensor Solutions for Italy (2013). [Online]. Available: http://www.eas.slu.edu/eqc/eqc_mt/MECH.IT/
- [9] RCMT (2013). [Online]. Available: <http://www.bo.ingv.it/RCMT/searchRCMT.html>
- [10] TDMT (2013). [Online]. Available: <http://cnt.rm.ingv.it/tdmt.html>
- [11] E. Guidoboni, G. Ferrari, D. Mariotti, A. Comastri, G. Tarabusi, and G. Valentini, *CFTI4Med, Catalogue of Strong Earthquakes in Italy (461 B.C.-1997) and Mediterranean Area (760 B.C.-1500)*. INGV-SGA, 2007, <http://storing.ingv.it/cfti4med/>
- [12] A. Rovida, R. Camassi, P. Gasperini, and M. Stucchi, Eds. *CPTI11, the 2011 Version of the Parametric Catalogue of Italian Earthquakes*. Milano, Bologna, 2011, <http://emidius.mi.ingv.it/CPTI>, doi: 10.6092/INGV.IT-CPTI11.
- [13] A. Frepoli and A. Amato, "Contemporaneous extension and compression in the northern Apennines from earthquake fault-plane solutions," *Geophys. J. Int.*, vol. 129, pp. 368–388, 1997.
- [14] A. Tertuliani and A. Maramai, "Macroseismic evidences and site effects for the Lunigiana (Italy) 1995 earthquake," *J. Seismol.*, vol. 2, pp. 209–222, 1998.
- [15] B. Castello, G. Selvaggi, C. Chiarabba, and A. Amato, *CSI Catalogo della sismicità italiana 1981–2002, versione 1.1*. Roma: INGV-CNT, 2006, <http://csi.rm.ingv.it/>
- [16] Servizio Geologico d'Italia, *Progetto CARG, Carta Geologica d'Italia, scale 1:50,000, Sheets 233 Pontemoli, 248 La Spezia, 249 Massa Carrara*. ISPRA, 2013, <http://www.isprambiente.gov.it/Media/carg/liguria.html>
- [17] A. Argnani, G. Barbacini, M. Bernini, F. Camurri, M. Ghielmi, G. Papani, F. Rizzini, S. Rogledi, and L. Torelli, "Gravity tectonics driven by Quaternary uplift in the Northern Apennines: insights from the La Spezia-Reggio Emilia geo-transect," *Quatern. Int.*, vol. 101–102, pp. 13–26, 2003.
- [18] F. Brozzetti, P. Boncio, D. Di Naccio, G. Lavecchia, D. P. Tinari, L. Torelli, M. Bernini, E. Eva, and S. Solarino, "A multidisciplinary approach to the seismotectonics of the Lunigiana and Garfagnana extensional basins (northern Tuscany, Italy)," *Rend. Soc. Geol. It.*, vol. 5, pp. 88–89, 2007.
- [19] R. Basili, G. Valentini, P. Vannoli, P. Burrato, U. Fracassi, S. Mariano, M. M. Tiberti, and E. Boschi, "The database of individual seismogenic sources (DISS), version 3: summarizing 20 years of research on Italy's earthquake geology," *Tectonophysics*, vol. 453, no. 1–4, pp. 20–43, 2008, doi: 10.1016/j.tecto.2007.04.014.
- [20] M. Bernini and G. Papani, "La distensione della fossa tettonica della Lunigiana nord-occidentale," *Boll. Soc. Geol. Ital.*, vol. 121, pp. 313–341, 2002.
- [21] D. Di Naccio, P. Boncio, F. Brozzetti, F. J. Pazzaglia, and G. Lavecchia, "Morphotectonic analysis of the Lunigiana and Garfagnana grabens (northern Apennines, Italy): Implications for active normal faulting," *Geomorphology*, vol. 201, pp. 293–311, 2013.
- [22] L. Pierotti, F. Botti, S. Bracaloni, I. Burrelli, M. Cattaneo, and F. Gherardi, "Hydrogeochemistry of Magra Valley (Italy) aquifers: geochemical background of an area investigated for seismic precursors," *Proc. Earth Planet. Sci.*, vol. 7, pp. 697–700, 2013.
- [23] A. Castellarin, C. Eva, G. Giglia, G. B. Vai, E. Rabbi, G. A. Pini, and G. Crestana, "Analisi strutturale del Fronte Appenninico Padano," *Giorn. Geol.*, vol. 3a, no. 47, pp. 1–2, 1985.
- [24] R. Bürgmann, P. A. Rosen, and E. J. Fielding, "Synthetic aperture radar interferometry to measure Earth's surface topography and its deformation," *Ann. Rev. Earth Planet. Sci.*, vol. 28, pp. 169–209, 2000.
- [25] S. Stramondo, "The Tohoku–Oki earthquake: A summary of scientific outcomes from remote sensing," *IEEE Geosci. Remote Sens. Lett.*, vol. 10, no. 4, pp. 895–897, Jul. 2013.
- [26] E. Papageorgiou, M. Fomelis, and I. Parcharidis, "Long- and short-term deformation monitoring of Santorini Volcano: Unrest evidence by DInSAR

- analysis," *IEEE J. Sel. Topics Appl. Earth Observ. Remote Sens.*, vol. 5, no. 5, pp. 1531–1537, Oct. 2012.
- [27] L. Tao, H. Zhang, C. Wang, and Y. Tang, "Ground deformation retrieval using Quasi coherent targets DInSAR, with application to suburban area of Tianjin, China," *IEEE J. Sel. Topics Appl. Earth Observ. Remote Sens.*, vol. 5, no. 3, pp. 867–873, Jun. 2012.
- [28] K. A. C. de Macedo, C. Wimmer, T. L. M. Barreto, D. Lubeck, J. R. Moreira, L. M. L. Rabaco *et al.*, "Long-term airborne DInSAR measurements at X- and P-bands: A case study on the application of surveying Geohazard threats to pipelines," *IEEE J. Sel. Topics Appl. Earth Observ. Remote Sens.*, vol. 5, no. 3, pp. 990–1005, Jun. 2012.
- [29] F. Covelto, F. Battazza, A. Coletta, E. Lopinto, C. Florentino, L. Pietranera, G. Valentini, and S. Zoffoli, "CSK an existing opportunity for observing the Earth," *J. Geodynam.*, vol. 49, pp. 171–180, 2010.
- [30] U. Wegmuller and C. Werner, "Gamma SAR processor and interferometry software," in *Proc. 3rd ERS Symp. Space Service Environ.*, Florence, Italy, 1997.
- [31] R. Goldstein and C. Werner, "Radar interferogram filtering for geophysical applications," *Geophys. Res. Lett.*, vol. 25, no. 21, pp. 4035–4038, 1998.
- [32] M. Costantini, "A novel phase unwrapping method based on network programming," *IEEE Trans. Geosci. Remote Sens.*, vol. 36, no. 3, pp. 813–821, 1998.
- [33] Y. Okada, "Internal deformation due to shear and tensile faults in a half space," *Bull. Seismol. Soc. Am.*, vol. 82, pp. 1018–1040, 1992.
- [34] R. Hanssen, *Radar Interferometry: Data Interpretation and Error Analysis*. New York, NY, USA: Springer-Verlag, 2001.
- [35] S. Kirkpatrick, C. D. Gelatt, and M. P. Vecchi, "Optimization by simulated annealing," *Science*, vol. 220, no. 4598, pp. 671–680, May 1983.
- [36] W. Menke, *Geophysical Data Analysis: Discrete Inverse Theory*. New York, NY, USA: Academic, pp. 289, 1989.
- [37] B. Hernandez, F. Cotton, and M. Campillo, "Contribution of radar interferometry to a two-step inversion of the kinematic process of the 1992 Landers earthquake," *J. Geophys. Res.*, vol. 104, no. B6, pp. 13,083–13,099, 1999.
- [38] D. L. Wells and K. J. Coppersmith, "New empirical relationships among magnitude, rupture length, rupture width, area, and surface displacement," *Bull. Seismol. Soc. Amer.*, vol. 84, pp. 974–1002, 1994.
- [39] K. L. Feigl, "Estimating earthquake source parameters from geodetic measurements," in *International Handbook of Earthquake and Engineering Seismology*, vol. 81A, 2002, pp. 607–620.
- [40] R. L. Gawthorpe and J. M. Hurst, "Transfer zones in extensional basins; their structural styles and influence in drainage development and stratigraphy," *J. Geol. Soc.*, vol. 150, pp. 1137–1152, 1993.



Salvatore Stramondo (M'05–SM'14) received the laurea (M.S.) degree in electronic engineering from the University "La Sapienza," Rome, Italy, in 1996, and the Ph.D. degree in geoinformation from the University "Tor Vergata," Rome, Italy, in 2007.

He joined the Istituto Nazionale di Geofisica e Vulcanologia (INGV), Rome, Italy, in 1997, where he is currently Senior Researcher. He is Adjunct Professor of "Remote Sensing" and "Cartography and Topography" at the University of Calabria, Rende, Italy. He was Invited Researcher at the CNR-IRECE, Naples, Italy, in 1997; IGP, Paris, France, in 1998; JPL, Pasadena, CA, USA, in 2000; and IIT-Bombay, Bombay, India, in 2001. He is author of 50 international papers. He is Actually Coordinator of the APHoRISM FP7 Project and TERRAFIRMA Tectonic Theme GSE Project. He has been Chairman and Co-Chairman at several international conferences.

Dr. Stramondo is Editor of *Remote Sensing* journal and Associate Editor of IEEE TRANSACTIONS ON GEOSCIENCE AND REMOTE SENSING LETTERS. His research interests include SAR interferometry techniques and geophysical applications.



Paola Vannoli received the degree in geological sciences and the Ph.D. degree in earth sciences from Università degli Studi di Roma "La Sapienza," Rome, Italy, in 1994 and 2000, respectively.

She joined the Istituto Nazionale di Geofisica e Vulcanologia (INGV), Rome, Italy, in 2001, where she is currently Research Scientist. Since 2001, she has been working on identification and characterization of seismogenic sources using geological, seismological, and historical data. She is a member of the DISS Working Group (Database of Individual Seismogenic

Sources; <http://diss.rm.ingv.it/diss/>) and the Emergeo Working Group (emergency field surveying of surface earthquake effects; <http://emergeo.ingv.it/>). She is involved in Italian and international projects related to seismic hazard. Her research interest includes active tectonics and tectonic geomorphology.



Valentina Canelli received the degree in physics from University of Roma Tre, Rome, Italy, in 2000.

Since November 1, 2005, she has been a Researcher with Seismology and Tectonophysics Department, Istituto Nazionale di Geofisica e Vulcanologia (INGV), Rome, Italy. Her research interests include study of kinematics and source geometries of giant earthquakes through linear and nonlinear joint inversion of multiple data type (tide-gages, satellite altimetry, and GPS recordings), analysis of the associated slip distribution and computation of the Coulomb Failure Function (CFF) variation on a possible aftershock plane, analysis and development on numerical and semi-analytic algorithms for the study of the global effects of giant earthquakes, computation of global coseismic and postseismic deformation through the simulation of elastic and viscoelastic response to a seismic dislocation, application of the Post-Widder Laplace inversion algorithm postseismic rebound models, and comparative analysis of radon-222 time series acquired by prototype stations located in seismically active areas through the development of correlation numerical algorithms



Marco Polcari was born in Naples, Italy, in 1984. He received the Master's degree in telecommunication engineering from the University Federico II, Naples, Italy, in 2012. He is currently pursuing the Ph.D. degree in geophysics from the University of Bologna, Bologna, Italy.

He is currently working in SAR interferometry fields with the Istituto Nazionale di Geofisica e Vulcanologia (INGV) in Rome, Italy. His research interests include the analysis of the remote sensed data processed by Differential Interferometric SAR techniques (DInSAR), seismic and volcanic areas studying the deformation occurred during a coseismic event, and slow displacements characterizing the interseismic phase of an earthquake or the volcanoes temporal behavior by means of multi-temporal time series analysis.



Daniele Melini is a Researcher with the Seismology and Tectonophysics Department, Istituto Nazionale Geofisica e Vulcanologia (INGV), Rome, Italy.

His research interests include computational geodynamics with focus on numerical modeling of geodetic data for coseismic, postseismic, and postglacial processes.



Sergey Samsonov received the M.S. degree in physics from Moscow State University, Moscow, Russia, in 1999, and the Ph.D. degree in geophysics and environmental science from the Western University, London, ON, Canada, in 2007.

He is a Research Scientist with the Canada Centre for Mapping and Earth Observation, Natural Resources Canada specializing in high resolution and high precision measurement of ground deformation with Interferometric Synthetic Aperture Radar (InSAR) caused by earthquakes, landslides, volcanic eruptions, and anthropogenic subsidence due to mining and extraction of oil/gas, and groundwater.



Marco Moro received the laurea and Ph.D. degrees both in geology from the University "La Sapienza," Rome, Italy, in 1996 and 2007, respectively.

He joined the Istituto Nazionale di Geofisica e Vulcanologia (INGV) in 2000, where he is currently Researcher. He was an Invited Researcher with the CNR-IGAG, Rome, Italy, in 2004. He is author of more than 40 international papers, several contributions to National and International conferences. He is actually the task leader in National (MIUR "Progetto Premiale INGV Studio multidisciplinare della fase di preparazione di un terremoto"; Abruzzo Project) and International (FP7 MarSite) projects. His research interests include active tectonics by means of tectonic

geomorphology studies necessary to identify seismogenic sources (historical and instrumental seismicity analysis, stress field from data break-outs and focal mechanisms, recognition and mapping of tectonic features using photo interpretation, geological mapping, and analysis of DEM); paleoseismology approach aimed at the characterization of the geometric and kinematic behavior of the seismogenic structures; analyses and interpretation of coseismic deformations by means of DInSAR images; analyses and interpretation of interseismic deformations by means of multitemporal DInSAR time series; quaternary geology integrating the stratigraphic sequences to paleosurfaces for the geological reconstruction of the quaternary evolution in basins sectors; study of the deep gravitational slope deformations (DGPV) and their interaction with the active tectonics, through the integration of differential interferometry (DInSAR) and geomorphologic techniques.



Christian Bignami received the Laurea (M.S.) degree in telecommunications engineering from Sapienza University of Rome, Rome, Italy, in 2002, and the Ph.D. degree in electromagnetism, in June 2008.

Currently, he is member of the Remote Sensing Unit of the Istituto Nazionale di Geofisica e Vulcanologia (INGV) in Rome, Italy, and since 2002, he has been collaborating with the Department of Electronic Engineering, Sapienza University of Rome. He is involved in Italian and international projects supported by the European Commission, Civil Protection Department, European Space Agency. His research interest includes remote sensing applications for seismic and volcanic area monitoring by using Synthetic Aperture Radar (SAR) and optical very high resolution sensors, processing and analysis of satellite data by means of SAR interferometric techniques for surface deformation, and change detection and classification techniques of urban environment with very high-resolution optical data.



Michele Saroli received the Ph.D. degree in DST (Earth Science Department) from “La Sapienza” University of Rome, Rome, Italy.

He carried on studies for the definition of the Quaternary evolution of central Apennine basins defining active tectonic features. He conducted applied geological and geomorphological researches about edge-slope-valley bottom evolution system, taking into account tectonic and gravity relationship (DSGSD) by photogeology, morphotectonic analysis, paleoseismological studies, and interferometric data.

Currently, he is Research-Professor Adj. of “Geology” and “Applied geology for the environment” at DICeM-Department of Civil and Mechanical Engineering of Cassino and Southern Lazio University, Cassino Frosinone, Italy.